Management Strategies and Engineering Sciences 2026; 8(1):1-25

Monitoring Drought in the Lake Urmia Basin Using Global Precipitation Data

Edris Ahmad Ebrahimpour[1*]

[1] Department of Civil Engineering, Ur.C., Islamic Azad University, Urmia, Iran

*** Corresponding author email address**: ed.ahmadebrahimpour@iau.ac.ir

Received: 2025-03-01 **Reviewed:** 2025-04-17 **Revised:** 2025-04-24 **Accepted:** 2025-05-03 **Published:** 2026-02-01

Abstract

This study investigates the drought status in the Lake Urmia basin using the Standardized Precipitation Index (SPI) and the Standardized Precipitation-Evapotranspiration Index (SPEI) under current and climate change conditions. To monitor past drought events, observational data and precipitation records from global databases—namely CRU, GPCC, and UDEL—were utilized. The results of drought monitoring revealed that severe droughts occurred in the basin during the years 1989, 1991, between 1999 and 2001, and in 2008. Moreover, the evaluation of precipitation datasets for drought monitoring showed that the GPCC database performed best, followed by CRU and UDEL, respectively. Furthermore, to forecast future droughts, a hybrid model combining Support Vector Regression (SVR) and Genetic Algorithm (GA-SVR) was employed. The drought forecasting results indicated that prediction accuracy increases with the extension of the SPI calculation scale, whereas it decreases as the forecast lead time increases. To evaluate future droughts, outputs from 29 General Circulation Models (GCMs) were combined under both the optimistic RCP 2.6 and pessimistic RCP 8.5 scenarios. The evaluation of the hybrid model output demonstrated that temperature in the basin is projected to increase under both scenarios, while precipitation is expected to rise under the optimistic scenario and decrease under the pessimistic scenario. Future drought monitoring based on the SPI revealed that drought frequency will not significantly increase. However, the SPEI results indicated a statistically significant rise in the number of future drought events. The findings suggest that temperature will play a critical role in future drought occurrences. For instance, based on the nine-month SPEI, 12 severe drought events were recorded during the baseline period, whereas under the RCP 2.6 scenario, the number of events is projected to increase to 18, 19, and 19 during the near future (2011–2040), mid-century (2041–2070), and far future (2071–2100), respectively. Under the RCP 8.5 scenario, the corresponding figures are expected to rise to 21, 28, and 38 events, respectively.

Keywords: *Drought monitoring, drought forecasting, global precipitation database, climate change, Lake Urmia basin, support vector regression.*

How to cite this article:

Ebrahimpour, E. A. (2026). Monitoring Drought in the Lake Urmia Basin Using Global Precipitation Data. Management Strategies and Engineering Sciences, 8(1), 1-25.

1. Introduction

Drought as a multifaceted natural hazard has long posed severe challenges to environmental stability, economic resilience, and water resource sustainability in semi-arid regions of the world. With the intensification of global climate change, concerns regarding the increased frequency, severity, and duration of droughts have become central to hydrological and climate science discourses. Nowhere is this more pertinent than in fragile basins such as Lake Urmia, where hydrological imbalances can trigger cascading socio-environmental consequences. The Standardized Precipitation Index (SPI) and the Standardized Precipitation Evapotranspiration Index (SPEI) are widely acknowledged tools for drought monitoring and forecasting, providing temporal flexibility and climate sensitivity that make them effective across various spatial and temporal scales [1, 2]. This study responds to the pressing need for robust drought analysis under projected climate scenarios by integrating SPI

and SPEI indices with ensemble-based outputs of General Circulation Models (GCMs) and a hybrid GA-SVR forecasting model to evaluate drought dynamics in the Lake Urmia Basin under RCP 2.6 and RCP 8.5 pathways.

Historical and projected precipitation datasets form the cornerstone of reliable drought analyses, yet their quality and spatial resolution vary substantially across global datasets. Comparative studies have underscored the need for regional calibration to correct systematic biases inherent in gridded products [3, 4]. Research conducted across Iran has identified discrepancies in rainfall estimation among products such as CRU, GPCC, and CHIRPS, suggesting the necessity of cross-verification with ground-based observations [5-7]. Precipitation uncertainty directly affects drought prediction, particularly in arid and semi-arid regions, where even marginal errors in input data can amplify hydrological stress assessments. In this regard, the CHIRPS dataset, as well as GPCC Full Reanalysis and CRU TS3.10, have proven valuable due to their temporal continuity and assimilation of rain gauge data [8-10].

One of the main limitations of traditional drought indices like SPI is their exclusive reliance on precipitation inputs, which can downplay drought conditions exacerbated by rising evapotranspiration rates driven by temperature increases. The SPEI was developed to overcome this limitation by incorporating potential evapotranspiration (PET), thereby rendering it more sensitive to the hydrological impacts of global warming [2]. This is especially critical in the Lake Urmia Basin, where temperature has been observed to rise steadily over recent decades, intensifying drought even during periods of average precipitation. PET dynamics, influenced by both radiation and temperature anomalies, can shift the balance between water supply and demand, creating a latent drought signature that may be undetected by precipitation-only indices [11, 12].

Climate model projections indicate that warming trends in Iran will intensify through the 21st century, particularly under high-emissions scenarios like RCP 8.5. Increases in mean temperature, in conjunction with variability in precipitation patterns, are expected to extend the duration and magnitude of droughts. The inclusion of multiple future horizons—near-term (2011–2040), mid-century (2041–2070), and end-of-century (2071–2100)—allows for comparative evaluations across temporal frames, providing essential insights for long-term water resource management. Numerous studies have affirmed that temperature-induced intensification of drought outweighs the effects of moderate increases in precipitation, a trend that is captured more accurately in SPEI-based models [13, 14].

Forecasting drought events remains a pivotal goal in hydrology, and machine learning techniques, particularly those integrating statistical and evolutionary algorithms, offer significant advancements in prediction accuracy. The GA-SVR (Genetic Algorithm–Support Vector Regression) model used in this study exemplifies a hybrid approach that optimizes model parameters to enhance predictive performance, particularly for short-term drought forecasting based on SPI across different temporal scales. Prior work using neural networks and wavelet transformations has established the efficacy of hybrid models in capturing nonlinear relationships in climate time series [15-17]. Moreover, statistical validation has shown that the predictability of SPI improves with increasing aggregation timescales, whereas forecast accuracy declines with longer lead times—findings that align with this study's results [18].

As climate change exacerbates hydrometeorological variability, scenario-based drought forecasting becomes essential for risk mitigation and policy planning. RCP 2.6, representing a low-emission stabilization pathway, and RCP 8.5, representing a high-emission trajectory, capture the range of plausible futures and inform resilience-building strategies in water-stressed regions. Under RCP 2.6, precipitation in the Lake Urmia Basin is projected to increase modestly, while under RCP 8.5, significant declines in rainfall and substantial warming are expected, likely amplifying drought conditions. The divergence in drought projections between SPI and SPEI under both scenarios underscores the importance of incorporating temperature-sensitive indices into vulnerability assessments [19, 20]. Even under the optimistic RCP 2.6 scenario, the SPEI indicated a noticeable rise in the frequency of drought events, implying that warming trends alone, irrespective of rainfall improvements, can destabilize hydrological balances.

The relevance of these findings is particularly acute for basins undergoing anthropogenic stress and environmental degradation, such as Lake Urmia. The declining water levels in the lake, driven by both climatic and human-induced factors, have made it a symbol of Iran’s environmental vulnerability. Accurate, localized, and climate-sensitive drought predictions are thus critical to reversing or mitigating ecological collapse. Integrating both SPI and SPEI indices with GCM ensembles not only enhances model robustness but also provides multi-perspective diagnostics that support proactive water governance. In addition,

pedagogical and societal outreach components, such as increasing climate literacy among youth, can play a role in preparing communities for climate-induced water challenges [21, 22].

Furthermore, the implications of this study go beyond hydrology and climate science and extend into the realms of economics, law, and institutional responsibility. Climate-related drought impacts on agricultural productivity, public health, and biodiversity place a moral and legal obligation on national and international institutions to ensure adaptive capacity and support mechanisms, especially for vulnerable regions [23, 24]. The findings here contribute to this broader conversation by quantifying risks and offering actionable knowledge rooted in scientific analysis and future scenario planning.

In conclusion, this study is a response to the growing imperative to bridge the gap between observed drought patterns, climate projections, and early warning systems. By employing a hybrid modeling framework that includes the GA-SVR algorithm, SPI and SPEI indices, and GCM outputs under RCP pathways, this research delivers an integrated assessment of current and future drought conditions in the Lake Urmia Basin. The results emphasize the increasing divergence between precipitation-only and temperature-sensitive indices in a warming climate, highlight the importance of scale in drought analysis, and stress the necessity of short-lead-time forecasting to improve regional water resource planning. As the consequences of climate change continue to unfold, such evidence-based studies will be crucial in guiding adaptive responses across policy, practice, and science.

2. Methodology

2.1. Study Area

In this study, monthly precipitation data from the Urmia synoptic station, located in the Lake Urmia watershed in northwestern Iran, were used for the period from 1984 to 2013. The Lake Urmia watershed, covering an area of approximately 51,862 square kilometers, includes nearly half of West Azerbaijan Province (21,072 km²), a large portion of East Azerbaijan Province (20,183 km²), and part of Kurdistan Province (5,320 km²). At a water level elevation of 1,275.86 meters (the 49-year average), Lake Urmia spans an area of 5,320 km², constituting about 10.25% of the entire watershed. Due to its geographical setting, the watershed receives relatively high levels of precipitation, primarily in the form of snow during winter. River flow data indicate that, on average, 64% of the inflow occurs in spring, 22.4% in autumn, 9.3% in winter, and only 4.3% in summer.

2.2. Data Used

To monitor drought, this study utilized precipitation data from 61 rain gauge stations within the watershed from 1984 to 2013. While there are numerous global precipitation databases, the focus of this study was on databases offering long-term precipitation records. Accordingly, the CRU, GPCC, and UDEL precipitation databases were reviewed, and the one with the best performance was used for drought calculation. These databases are introduced as follows:

CRU Precipitation Database

The Climatic Research Unit (CRU) at the University of East Anglia, UK, was established in 1972 and provides various climate datasets globally. CRU derives precipitation data by interpolating station-based observations. This study used the CRU TS 4.01 time series, which offers monthly precipitation data at a 0.5° × 0.5° spatial resolution, available from 1901 to 2016. Monthly CRU precipitation and temperature data from 1984 to 2013 were employed in this study. It is noteworthy that the temperature data were used to estimate potential evapotranspiration, which was required for drought monitoring. For further information, refer to Harris et al. (2014).

GPCC Precipitation Database

The Global Precipitation Climatology Centre (GPCC) was established in 1989 at the request of the World Meteorological Organization (WMO) and is operated by the German Meteorological Service. The GPCC provides monthly precipitation data at spatial resolutions of 2.5° × 2.5°, 1° × 1°, and 0.5° × 0.5°. Several versions of GPCC precipitation data have been released. In this study, version 7 of the reanalysis dataset with a 0.5° × 0.5° resolution was used. This dataset is based on precipitation records from 64,400 ground stations. Currently, GPCC data are available for the period from 1901 to 2013. For more details, see Schneider et al. (2015).

UDEL Precipitation Database

The University of Delaware (UDEL) provides global monthly temperature and precipitation data for researchers. UDEL collects station-based precipitation data from various sources, including the Global Historical Climatology Network, Environment Canada, the Hydrometeorological Institute in St. Petersburg (Russia), the Greenland Climate Network, and the National Center for Atmospheric Research

(NCAR). These data are converted into gridded precipitation data using the CAI interpolation method (Azizi et al., 2016). Four versions of the UDEL dataset have been released so far, with the fourth version covering the 1901–2014 period. This study used the fourth version of the dataset for the years 1984 to 2013. The spatial resolution is 0.5° × 0.5°. The dataset is accessible via [http://www.esrl.noaa.gov/psd/data/gridded/data.UDel_Air T_Precip.htm] (last accessed April 17, 2018).

Future Precipitation and Temperature Data from the Ensemble Model

As discussed in the climate change section, multiple models have simulated future precipitation and temperature scenarios. This study used the outputs of 29 Atmosphere-Ocean General Circulation Models (AOGCMs), averaged together in a technique known as the "Ensemble" method. Monthly precipitation data for all individual models and the ensemble model at a 1° × 1° spatial resolution were obtained from [http://climate-scenarios.canada.ca/?page=gridded-data] (last accessed April 17, 2018). These outputs were downscaled using a proportional method.

2.3. Drought Indices

Standardized Precipitation Index (SPI)

McKee et al. (1993) developed the Standardized Precipitation Index (SPI) to monitor drought conditions in Colorado. This index is calculated by fitting a probability distribution function to precipitation data and transforming the resulting probability values into a standard normal distribution. SPI requires only precipitation data and can be computed at various time scales, including 1-, 3-, 6-, 9-, 12-, 24-, and even 48-month intervals. The key issue in SPI computation is the appropriate fitting of a statistical distribution to the precipitation data. Empirical evidence indicates that the gamma distribution is suitable for this purpose, though alternative distributions should not be dismissed without proper evaluation. After computing the SPI, drought conditions can be assessed using Table 1. As shown, a drought event occurs when the SPI is persistently negative, while severe drought is defined by an SPI value equal to or less than −1. A positive SPI value indicates the end of a drought.

Table 1. Drought Severity Classification Based on SPI Values

SPI Index Range	Drought Condition	D-Scale
−0.49 to 0.49	Normal	WD
−0.50 to −0.79	Mild Drought	D0
−0.80 to −1.29	Moderate Drought	D1
−1.30 to −1.59	Severe Drought	D2
−1.60 to −1.99	Very Severe Drought	D3
−2.00 or less	Exceptional Drought	D4

Standardized Precipitation-Evapotranspiration Index (SPEI)

Vicente-Serrano et al. (2010) introduced the SPEI index, emphasizing that temperature is also a critical parameter in drought conditions. The steps for calculating this index are exactly similar to those of the SPI, with the difference that, instead of relying solely on precipitation, the calculations are based on the difference between precipitation and potential evapotranspiration. Similar to the recommendations made for the SPI, Stagge et al. (2015) suggested that the GEV, normal, and Pearson Type III probability distributions be evaluated when calculating the SPEI. The *SPEI* package in the R software can be used to compute SPEI based on several common distributions (Beguería & Vicente-Serrano, 2013). To calculate potential evapotranspiration (PET), the Thornthwaite method was used. This method requires only temperature data and uses the following equations:

Equation (1): $\mathrm{PET} = 16\mathrm{K}\left(\frac{10\mathrm{T}}{\mathrm{I}}\right)^{\mathrm{m}}$

Equation (2): $I = \sum_{i=1}^{12}\left(\frac{T_i}{5}\right)^{1.514}$

Equation (3): $m = 6.75 \times 10^{-7} I^3 - 7.71 \times 10^{-5} I^2 + 1.79 \times 10^{-2} I + 0.492$

In these equations, *PET* represents monthly potential evapotranspiration in millimeters, *K* is the correction coefficient for the month and latitude, *T* is the average monthly temperature in degrees Celsius, *I* is the monthly heat index, and *m* is an empirical coefficient derived from *I*. The values of the correction coefficient *K* for the Lake Urmia basin are provided in the table below.

Table 2. Monthly correction coefficient (K) in the Thornthwaite equation for the Urmia Basin

Month	Jan	Feb	Mar	Apr	May	Jun	Jul	Aug	Sep	Oct	Nov	Dec

K	0.87	0.85	1.03	1.09	1.21	1.21	1.23	1.16	1.03	0.97	0.86	0.85

2.4. Drought Forecasting

In this study, the Support Vector Regression (SVR) method was used to monitor drought. Based on prior research, this method is recognized as effective for forecasting purposes. The method is explained in detail below.

Support Vector Regression Model and Genetic Algorithm

The SVR, a regression-based form of Support Vector Machine (SVM), was used in this study to forecast drought conditions. Determining the optimal values for SVR parameters through trial and error typically does not yield the highest accuracy. Therefore, the use of a metaheuristic algorithm to find optimal parameter values can enhance model performance. Consequently, the Genetic Algorithm (GA) was employed in this study to identify the appropriate parameter values. This algorithm is elaborated upon in the following sections.

2.5. Evaluation Criteria

In several parts of this study, criteria were needed to evaluate the performance of precipitation databases and the forecasting model. The following indicators were used: correlation coefficient (CC), root mean square error (RMSE), mean absolute error (MAE), and bias.

Equation (4):

$$CC = \frac{\frac{1}{n}\sum_{i=1}^{n}(y_i - \overline{y})(\hat{y}_i - \overline{\hat{y}})}{\sqrt{\frac{1}{n}\sum_{i=1}^{n}(y_i - \overline{y})^2}\sqrt{\frac{1}{n}\sum_{i=1}^{n}(\hat{y}_i - \overline{\hat{y}})^2}}$$

Equation (5):

$$RMSE = \sqrt{\frac{1}{n}\sum_{i=1}^{n}(y_i - \hat{y}_i)^2}$$

Equation (6):

$$MAE = \frac{1}{n}\sum_{i=1}^{n}|y_i - \hat{y}_i|$$

Equation (7):

$$Bias = \frac{\sum_{i=1}^{n}\hat{y} - \sum_{i=1}^{n}y}{\sum_{i=1}^{n}y} \times 100$$

Equation (8):

$$NSE = 1 - \frac{\sum_{t=1}^{T}(y_t - \hat{y}_t)^2}{\sum_{t=1}^{T}(y_t - \overline{y}_t)^2}$$

In the above formulas, y is the observed value, $\hat{y}$ is the estimated value, i is the monthly index, and n is the time series length. In addition to the above criteria, the Critical Success Index (CSI) was also used to evaluate the performance of precipitation databases in drought monitoring. This index is defined as follows (Wilks, 2011):

Equation (9):

$$CSI = \frac{H}{F + M + H} \times 100$$

In this equation, H is the number of correctly identified drought classes (i.e., instances where the drought class based on observed data matches the class based on database data), F is the number of incorrectly identified drought classes, and M is the number of drought events misclassified or undetected by the database (i.e., differences not in class but in whether drought was detected as normal or wetter, or vice versa). The optimal value for the CSI is 100 percent. According to Wilks (2011) and Boroujerdy-Katirai et al. (2016), an SPI value less than −0.5 is considered the threshold for drought occurrence in CSI calculations.

3. Findings and Results

3.1. Evaluation of Global Precipitation Databases and Their Performance in Drought Monitoring

Since the accuracy of drought monitoring depends on the quality of input data used to calculate drought indices, this section initially evaluates the accuracy of precipitation data from the selected databases. Figure 1 shows the precipitation regime in the Lake Urmia basin based on observed data and global databases. According to Figure 1-a, all databases generally overestimate monthly precipitation, although they successfully capture the overall precipitation regime. The observed average annual precipitation was 324 millimeters, while CRU, GPCC, and UDEL estimated it at 367 mm, 365 mm, and 360 mm, respectively. Figure 1-b presents the precipitation regime as a percentage. According to this figure, the GPCC database most closely aligns with the observed precipitation regime. Based on Figure 1, although UDEL provides a more accurate estimate of annual precipitation (Figure 1-a), it performs the worst in capturing the seasonal precipitation regime (Figure 1-b).

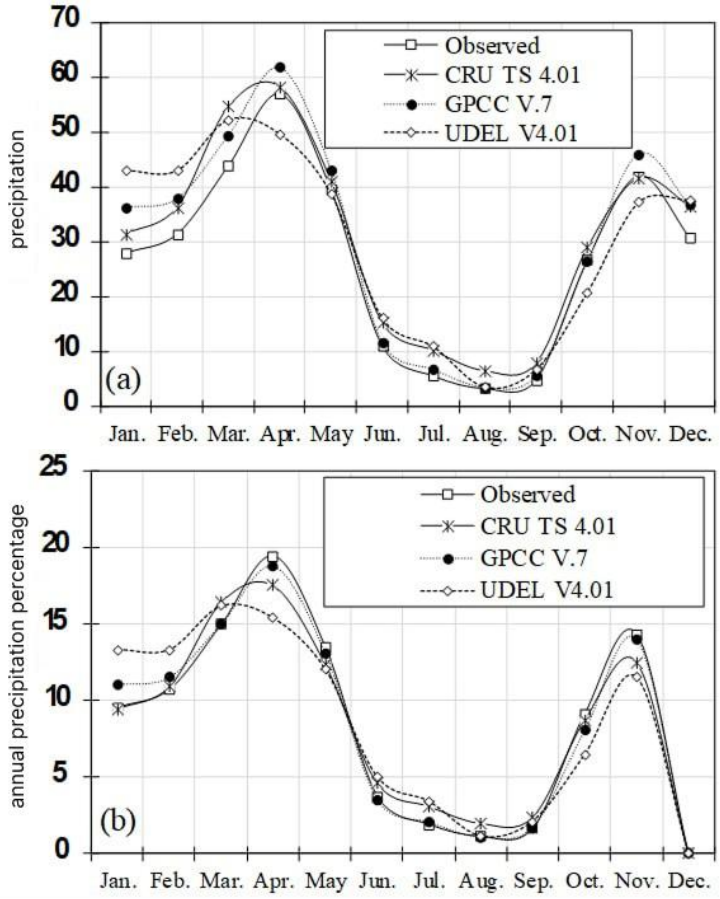

Figure 1. Precipitation regime in the Lake Urmia basin in millimeters and percentage

Figure 2 presents scatter plots of observed monthly precipitation versus monthly precipitation from different global databases, along with the empirical cumulative distribution function (eCDF). Overall, CRU tends to overestimate precipitation at a given probability level. This pattern of overestimation is also seen in the GPCC and UDEL plots. Figure 2-b shows that GPCC performs well in estimating precipitation in the Lake Urmia basin, with most data points falling close to the 1:1 line ($y = x$). UDEL, however, demonstrates the weakest performance, often overestimating or underestimating monthly precipitation. In summary, GPCC was found to be the best-performing database, with a coefficient of determination (R^2) of 0.95. CRU ranked second with $R^2 = 0.87$, and UDEL ranked last with $R^2 = 0.68$.

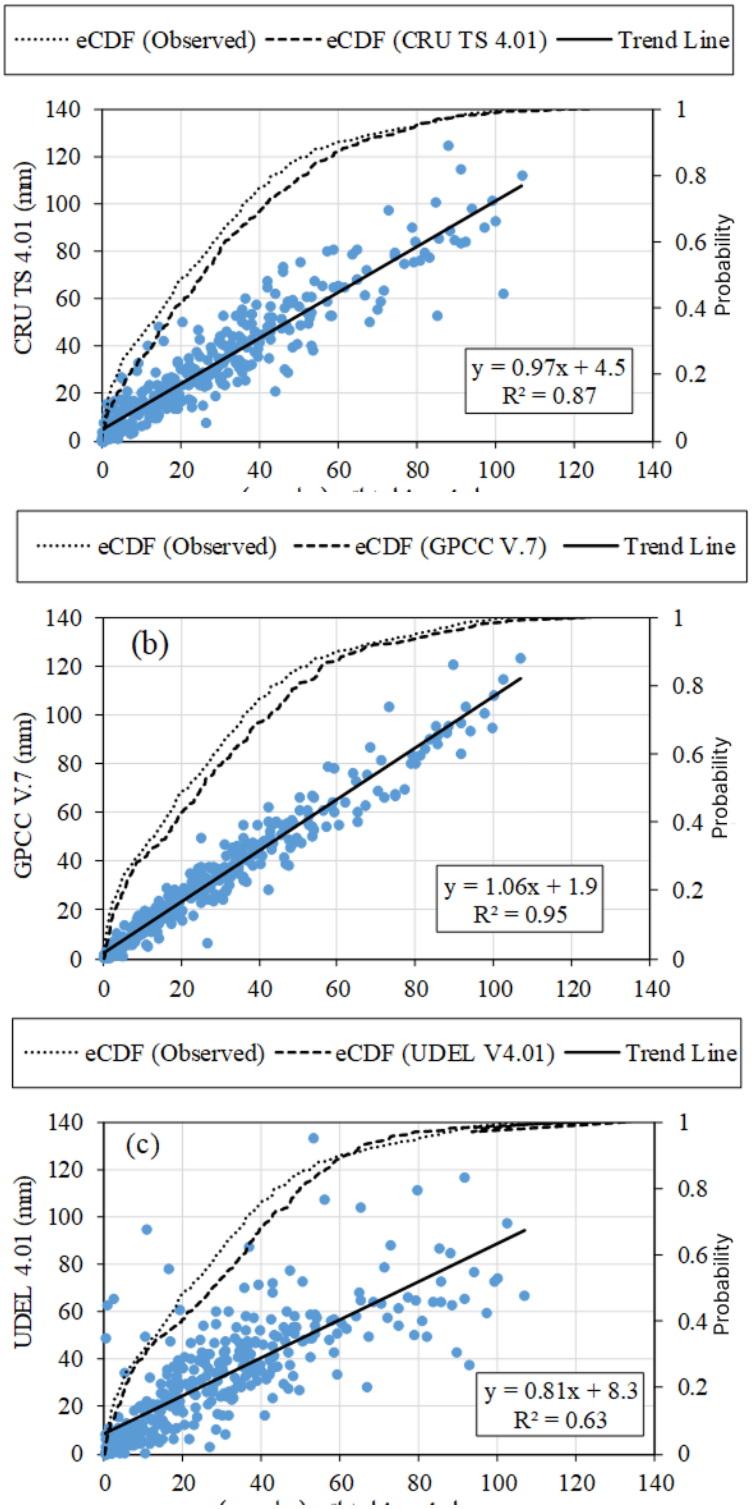

Figure 2. Scatterplots comparing global precipitation databases with observed precipitation, including cumulative distribution function (CDF) plots

For further evaluation, four performance metrics—CC, NSE, RMSE, and Bias—were calculated for all databases and for each month (Table 3). The results showed that, across various criteria, GPCC performed better than CRU and UDEL. The average CC for GPCC was 0.95, while it was 0.86 for CRU and 0.62 for UDEL. Bias analysis indicated that CRU and GPCC consistently overestimated precipitation in all months (except November for CRU and

October for GPCC), whereas UDEL underestimated precipitation in four months. The evaluation of the NSE metric showed that GPCC's data had significantly better accuracy than the others, with an average NSE of 0.81 compared to 0.05 and −1.06 for CRU and UDEL, respectively. Furthermore, the RMSE for GPCC was 1.5 and 2.5 times lower than that for CRU and UDEL, respectively.

Table 3. Monthly performance metrics for the studied precipitation databases

Database	Criteria	Jan	Feb	Mar	Apr	May	Jun	Jul	Aug	Sep	Oct	Nov	Dec
CRU	CC	0.84	0.87	0.84	0.87	0.92	0.95	0.65	0.71	0.85	0.97	0.92	0.90
	NSE	0.47	0.61	0.15	0.73	0.84	0.71	−1.99	−3.67	0.30	0.92	0.85	0.64
	RMSE (mm)	9.46	8.54	14.01	12.69	9.68	6.00	9.29	7.93	5.90	7.03	10.43	11.52
	Bias (%)	12.35	15.56	24.53	2.28	4.03	38.56	83.64	98.01	62.90	8.50	−1.09	18.63
GPCC	CC	0.95	0.95	0.90	0.98	0.98	0.94	0.97	0.90	0.94	0.98	0.97	0.96
	NSE	0.47	0.66	0.67	0.91	0.93	0.88	0.88	0.80	0.86	0.95	0.89	0.77
	RMSE (mm)	9.41	7.95	8.69	7.15	6.29	3.88	1.83	1.64	2.67	5.28	8.80	9.22
	Bias (%)	29.80	20.68	12.67	8.51	9.06	4.85	20.77	6.98	16.90	−0.77	9.51	19.15
UDEL	CC	0.57	0.54	0.48	0.72	0.77	0.46	0.14	0.61	0.41	0.93	0.80	0.95
	NSE	−1.36	−1.53	−0.43	0.39	0.58	−1.42	−10.34	0.16	−0.96	0.81	0.60	0.74
	RMSE (mm)	19.92	21.74	18.13	19.14	15.75	17.29	18.08	3.36	9.83	10.82	16.90	9.80
	Bias (%)	53.90	36.97	19.12	−12.75	−1.70	46.93	98.06	11.57	41.91	−21.68	−11.46	22.42

Precipitation analysis revealed that all databases contain errors in estimating precipitation amounts. However, the GPCC database has strong potential to serve as a substitute for observed precipitation in the Lake Urmia basin. The findings of Koutsouris et al. (2016), who evaluated GPCC, CRU, and UDEL in Tanzania, also confirmed that GPCC was the most accurate database, aligning with this study's results. However, in their study, UDEL outperformed CRU, a finding that diverges from this research and can be attributed to differences in input data and interpolation methods. The results of Alkenawi and Meksib (2016) in Saudi Arabia indicated that GPCC, CRU, and UDEL ranked first to third in terms of performance, which is consistent with the findings for the Urmia basin. Furthermore, the dominant error in global precipitation databases in the Urmia basin was Bias error, consistent with the findings of Adam & Lettenmaier (2003), Khalili & Rahimi (2014), and Funk et al. (2015).

Following precipitation evaluation, the drought monitoring capability of the precipitation databases was assessed. This phase used observed data, raw database outputs, and Bias-corrected (BC) global precipitation data. Figure 3 presents the SPI time series at 3-, 6-, 9-, and 12-month scales. According to Figure 3, the difference between observed SPI values and those derived from precipitation databases becomes more pronounced as the SPI timescale increases. The UDEL database showed significant deviations from observed SPI data during 1990, 1992–1996, and 2010–2011. In contrast, no significant differences were found in the SPI time series of GPCC and CRU. Drought monitoring based on observational and global data for the Urmia basin between 1984 and 2013 identified the most severe droughts in 1989, 1991, 1999–2001, and 2008, with the 1999–2001 drought being the longest and most intense.

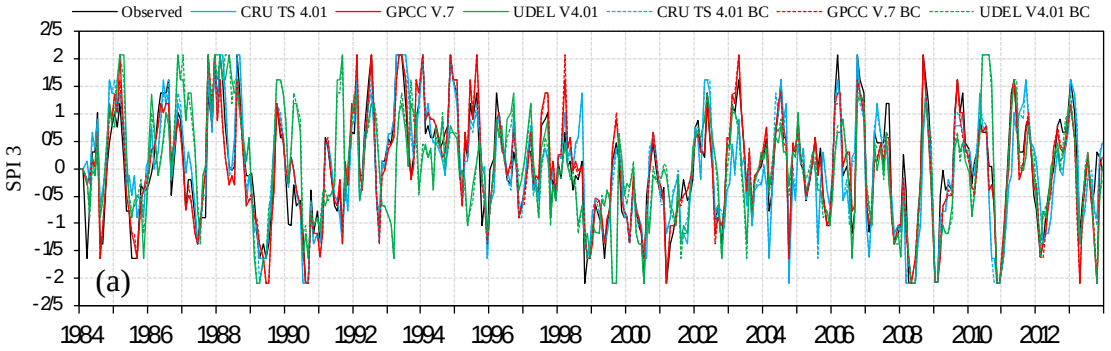

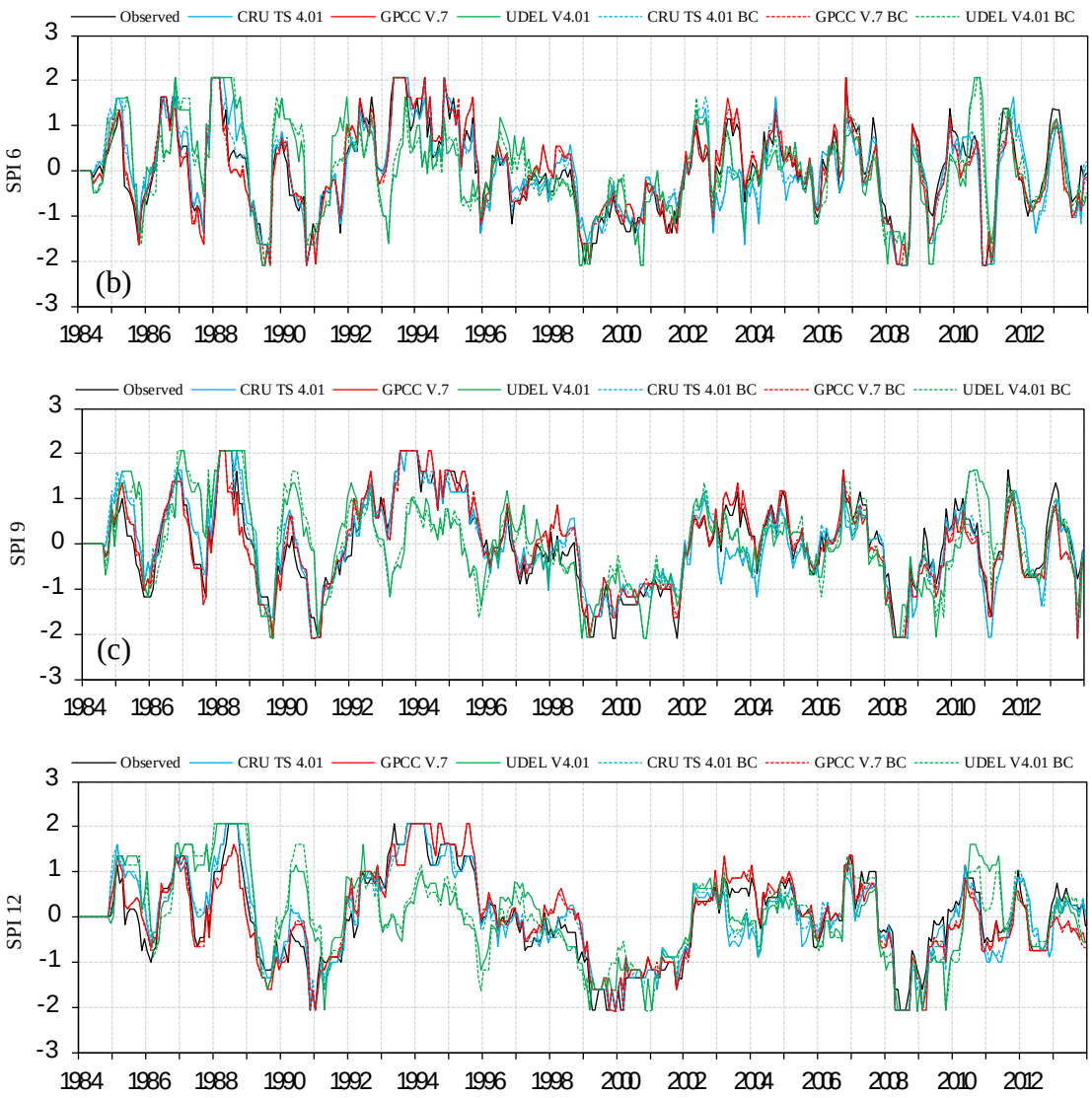

Figure 3. SPI time series at different temporal scales based on observed and global precipitation data

Table 4 presents the performance metrics of the studied precipitation databases across SPI scales of 3, 6, 9, and 12 months. Overall, the performance of global precipitation datasets improved with longer SPI timescales. For example, the CC, NSE, and RMSE for CRU at SPI-3 were 0.86, 0.71, and 0.52, respectively, improving to 0.92, 0.84, and 0.39 at SPI-12. Comparing raw and Bias-corrected data reveals only slight improvements. For instance, the NSE values for GPCC at SPI-3, SPI-6, SPI-9, and SPI-12 were 0.86, 0.91, 0.90, and 0.88 for raw data, and improved to 0.87, 0.92, 0.91, and 0.89 after Bias correction.

Table 4. Performance metrics of precipitation datasets at different SPI scales

Dataset	CC				NSE				RMSE			
	SPI 3	SPI 6	SPI 9	SPI 12	SPI 3	SPI 6	SPI 9	SPI 12	SPI 3	SPI 6	SPI 9	SPI 12
CRU TS 4.01	0.86	0.91	0.91	0.92	0.71	0.82	0.82	0.84	0.52	0.42	0.41	0.39
GPCC V.7	0.93	0.95	0.95	0.94	0.86	0.91	0.90	0.88	0.36	0.29	0.31	0.33
UDEL V4.01	0.66	0.68	0.66	0.65	0.33	0.36	0.32	0.30	0.79	0.77	0.80	0.81
CRU TS 4.01 BC	0.86	0.92	0.91	0.93	0.72	0.83	0.82	0.85	0.51	0.39	0.40	0.37
GPCC V.7 BC	0.93	0.96	0.95	0.95	0.87	0.92	0.91	0.89	0.35	0.28	0.29	0.31
UDEL V4.01 BC	0.67	0.71	0.68	0.66	0.34	0.42	0.37	0.33	0.78	0.74	0.77	0.79

To deepen the analysis, the CSI index was also calculated across all SPI timescales and for all databases in both raw and Bias-corrected formats (Table 5). Among all databases, GPCC had the best performance, correctly identifying at least 73% of drought events, with SPI-6 reaching 88%. The largest improvement after Bias correction was observed for GPCC at SPI-9, where CSI improved by 5%. Following GPCC, CRU ranked second in performance. UDEL showed the weakest capability for drought monitoring in the Urmia basin, with a maximum CSI of 59%, compared to 88% for CRU and 76% for GPCC.

Table 5. CSI values for precipitation datasets at different SPI scales

Dataset	SPI 3	SPI 6	SPI 9	SPI 12
CRU TS 4.01	57	71	70	65
GPCC V.7	73	88	80	73
UDEL V4.01	49	55	59	52
CRU TS 4.01 BC	62	76	74	67
GPCC V.7 BC	74	88	85	74
UDEL V4.01 BC	46	55	58	55

The studies by Boroujerdi-Katirai et al. (2016) and Rezaei et al. (2011) showed that GPCC outperformed GLDAS, MERRA, and NCEP/NCAR for drought monitoring in Iran. The present findings also confirm that GPCC performs better than CRU and UDEL. Therefore, it can be concluded that GPCC is one of the most suitable alternatives to observed precipitation for conducting drought studies in the Lake Urmia basin.

3.2. Drought Forecasting Results

Figure 4 illustrates the variation in performance metrics for forecasting different SPI timescales. According to the figure, as the SPI calculation timescale increases, the forecasting accuracy also improves; the highest accuracy is associated with SPI-24, and the lowest with SPI-3. This can be attributed to the smoothing of the SPI time series as the timescale increases—at shorter timescales, the SPI series exhibits more abrupt fluctuations, while longer timescales result in smoother behavior. Based on the CC metric, the one-step-ahead forecasts for short-term droughts monitored by SPI-3 and SPI-6 had correlations of 0.52 and 0.65, respectively. For SPI-9, SPI-12, and SPI-24, the CC values were 0.72, 0.75, and 0.86, respectively. A declining trend in the CC index is clearly observed as the forecasting lead time increases. For instance, for SPI-12, the correlation dropped from 0.75 in the first lead time to 0.19 by the fourth.

Similar patterns were observed with the RMSE metric. The RMSE chart demonstrates a strictly increasing trend with longer forecast lead times. The one-step-ahead RMSE values ranged from 0.23 for SPI-24 to 0.75 for SPI-3. For two-step-ahead forecasts, RMSE increased from 0.37 (SPI-3) to 1.01 (SPI-24). The RMSE values for other SPI scales fall within this range. The NSE metric showed results similar to the previous two, with the exception that in the fourth-step-ahead forecasts, SPI-3 had higher predictive accuracy than SPI-6, SPI-9, and SPI-12. In one-step-ahead forecasting, NSE was above 0.5 for all SPI scales, indicating acceptable agreement between observed and predicted SPI time series. However, the NSE dropped below zero in three-step-ahead forecasts for SPI-3 and SPI-6, and in four-step-ahead forecasts for all SPI scales except SPI-24, reflecting poor prediction accuracy.

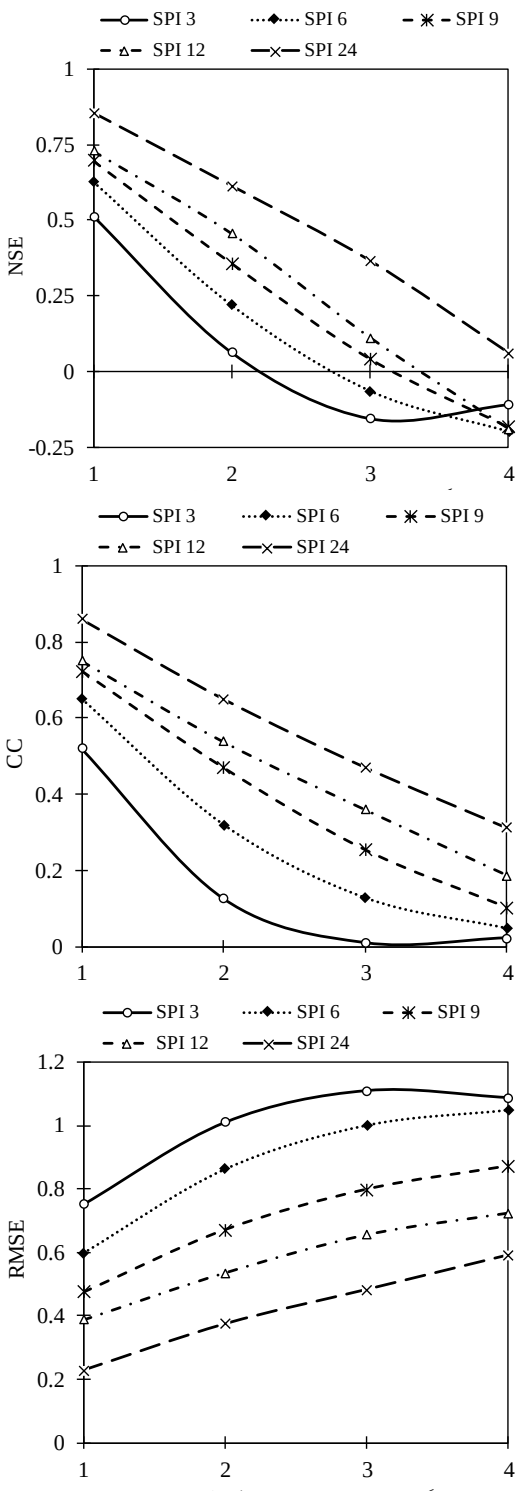

Figure 4. Variation of forecasting performance metrics from one to four months ahead

Figure 5 shows scatterplots of observed SPI-3 values versus predicted SPI-3 values for one- to four-step-ahead forecasts. In the one-step-ahead forecast, the model shows good accuracy, with data points clustered around the line y = x. However, as the forecast horizon extends, data points deviate further from the y = x line and become increasingly dispersed. In the fourth-step-ahead forecast, the data are nearly parallel to the x-axis (observed values), indicating a loss of correlation between observed and predicted values.

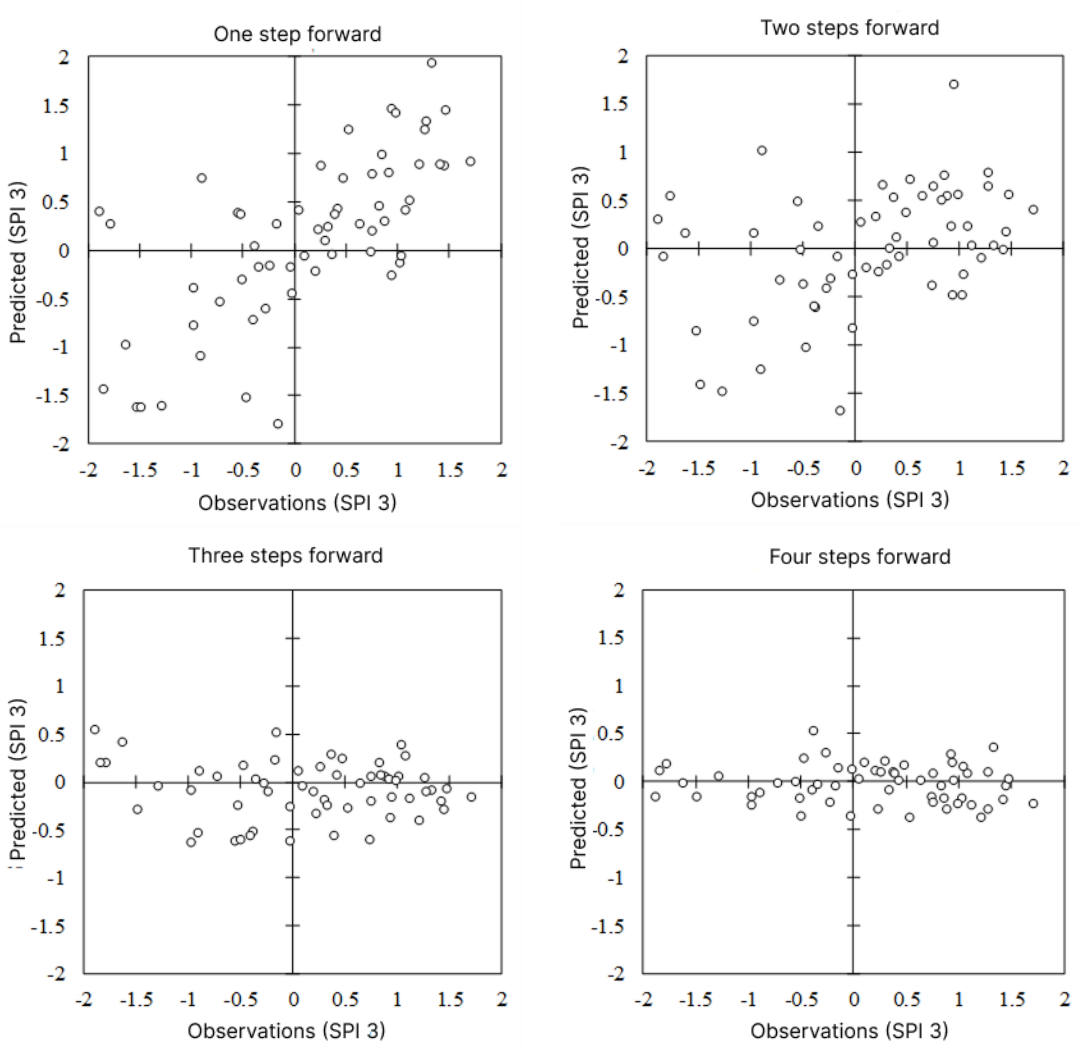

Figure 5. Scatterplot of SPI-3 forecasts using test data

Figure 6 displays observed and predicted SPI-6 values for lead times ranging from one to four steps ahead. Prediction accuracy is improved compared to SPI-3, yet the model still lacks sufficient forecasting power beyond the second lead step. In the one-step-ahead forecast, the model incorrectly classifies two drought events as wet conditions (data in the second quadrant) and two wet events as droughts (data in the fourth quadrant). In other cases, predictions are more accurate or have only minor discrepancies. Prediction errors in identifying wet and dry classes increase with lead time, and in the fourth-step-ahead forecast, nearly half of the drought events are predicted as wet, and vice versa. Thus, forecasting accuracy for longer lead times in SPI-6 remains suboptimal.

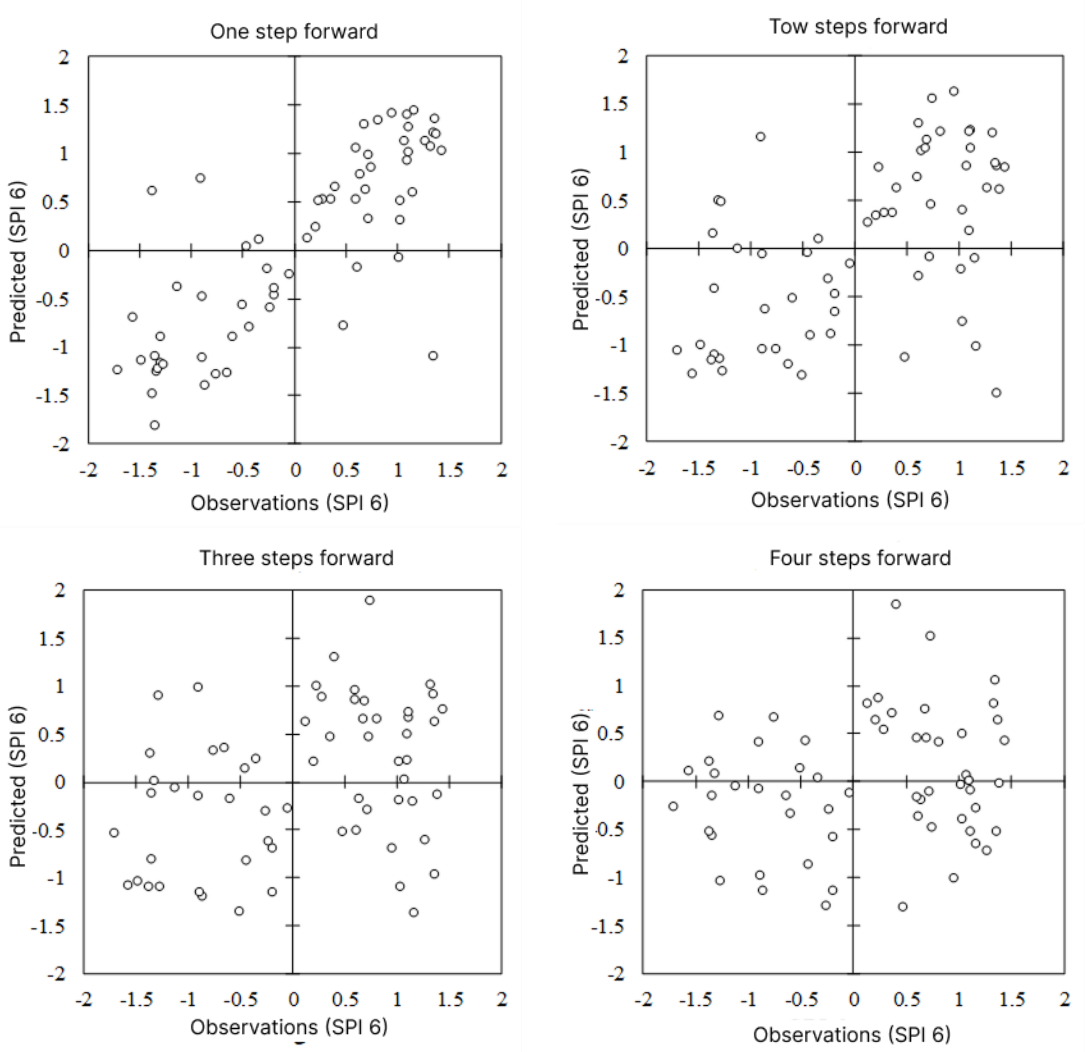

Figure 6. Scatterplot of SPI-6 forecasts using test data

Figure 7 presents observed and predicted SPI-9 values for lead times from one to four steps ahead. Forecasting accuracy has improved compared to SPI-3 and SPI-6. Up to two-step-ahead forecasts, no drought events are misclassified as wet, and most drought events (third quadrant) are accurately predicted up to the third lead step. However, forecast errors increase in the fourth-step-ahead, especially for normal conditions, which are predicted with less accuracy than drought conditions. As seen in prior figures, the one-step-ahead forecasts align closely with the y = x line, but by the fourth-step-ahead, data points are widely dispersed, indicating loss of correlation.

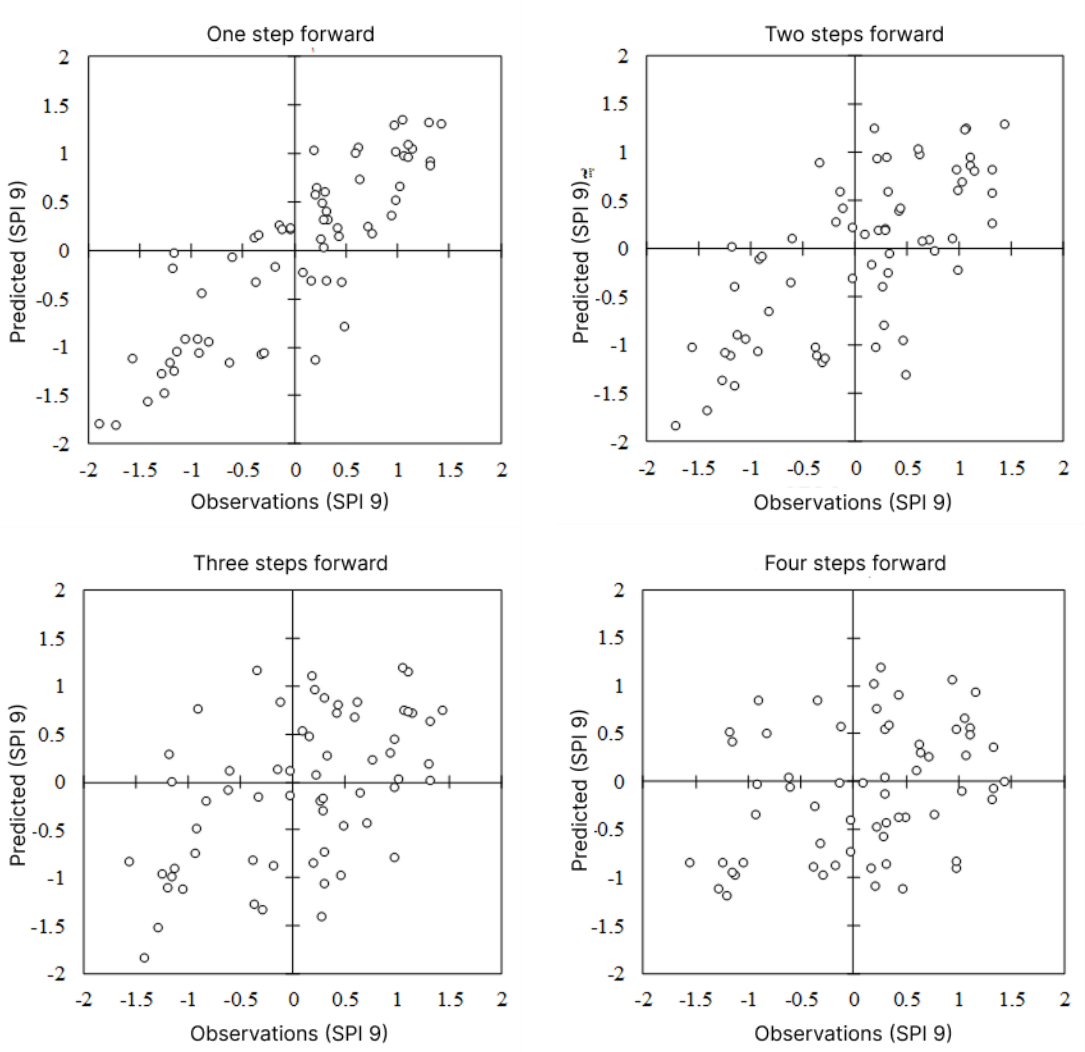

Figure 7. Scatterplot of SPI-9 forecasts using test data

Figure 8 shows scatterplots of observed versus predicted SPI-12 values for lead times from one to four steps ahead. While three-step-ahead forecasts remain relatively accurate, in the fourth-step-ahead forecast, data points are widely scattered across all quadrants, reflecting a significant reduction in correlation between observed and predicted values.

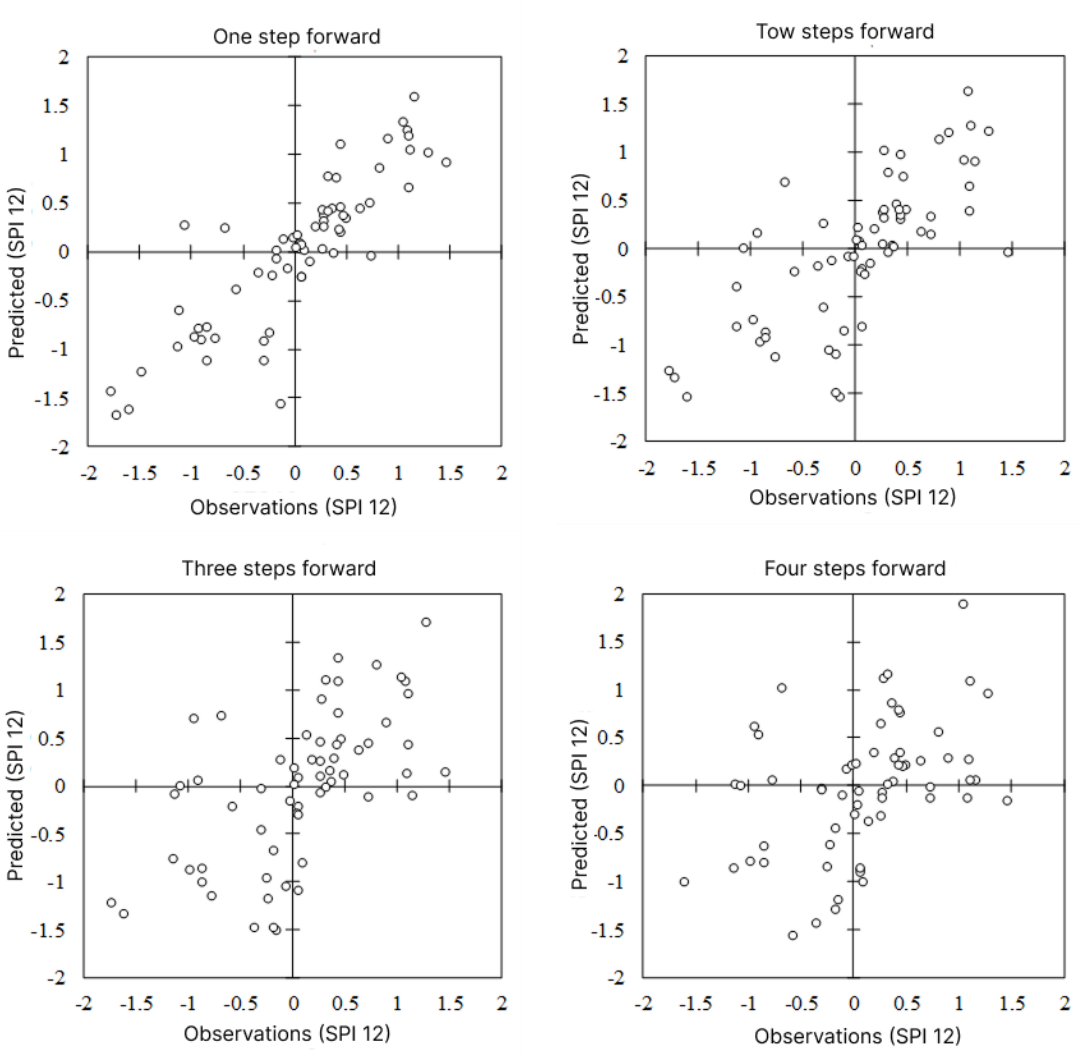

Figure 8. Scatterplot of SPI-12 forecasts using test data

Figure 9 displays the forecast results for SPI-24. In this figure, observed SPI-24 values are plotted against predicted values for one- to four-step-ahead forecasts. The SPI-24 model shows better accuracy than all shorter timescales. For example, in the one-step-ahead forecast, data points are more concentrated around the y = x line. However, in the fourth-step-ahead, points are scattered across all quadrants, indicating diminished correlation.

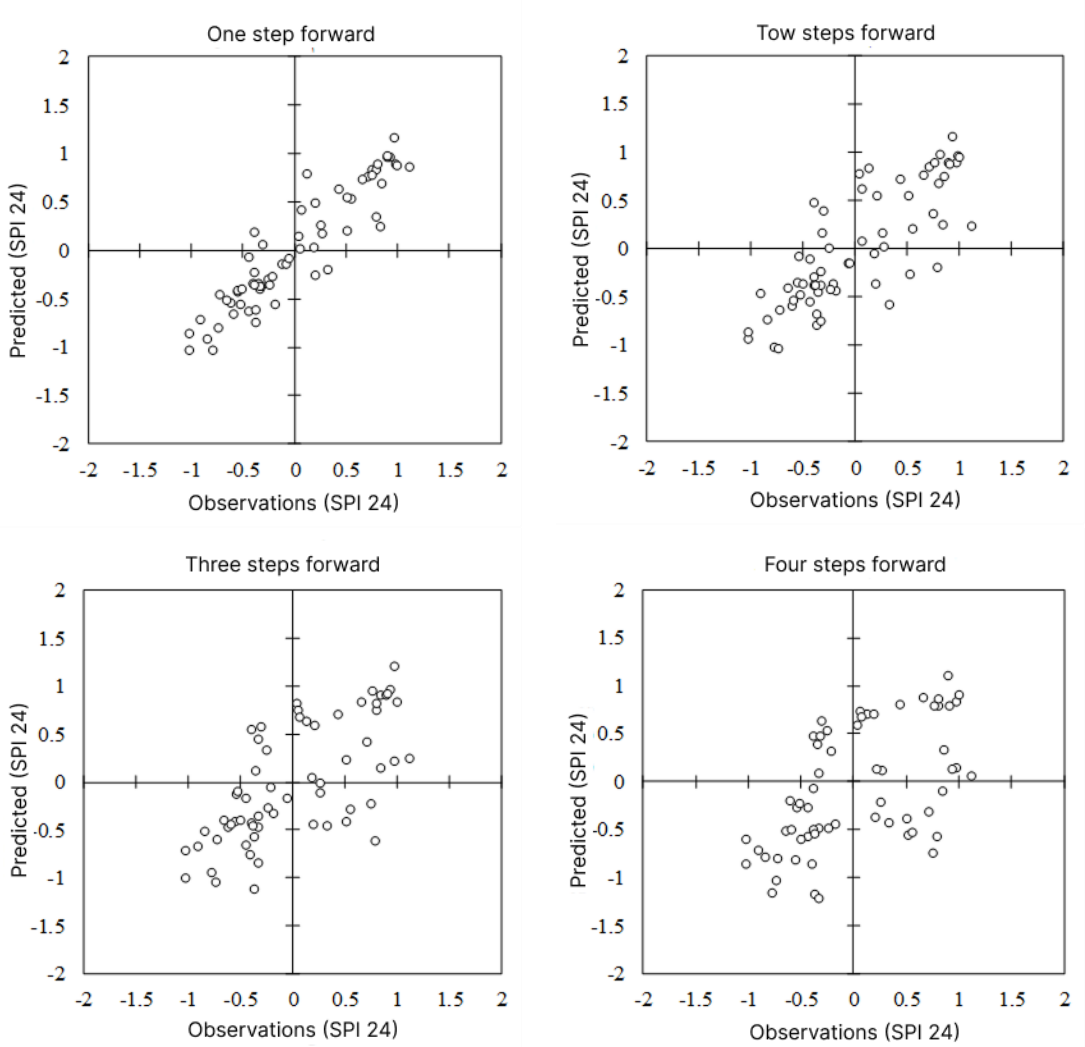

Figure 9. Scatterplot of SPI-24 forecasts using test data

The findings of this study are consistent with previous research using different drought forecasting methods. For instance, Mishra and Desai (2006) demonstrated that SPI forecasting accuracy improves with longer SPI timescales. Hosseini-Moghari and Araghi-Nejad (2015) investigated the effect of increasing lead times on forecast accuracy, finding that the best accuracy was achieved at one-month-ahead forecasts, with accuracy declining as lead time increased. This may be attributed to the changing behavior of SPI time series across lead times. At shorter scales, SPI exhibits high variability and can shift rapidly from extreme drought to wet conditions. In contrast, at higher scales, SPI shows smoother behavior with fewer fluctuations, indicating that drought or wet spells do not start or end abruptly.

3.3. Analysis of Temperature and Precipitation Changes in Future Periods

According to Figure 10, the average temperature during the baseline period was 10.36°C. Under the RCP 2.6 scenario, this average is projected to reach 10.90°C in the near future (2011–2040), 11.11°C in the mid-term future (2041–2070), and 11.08°C in the distant future (2071–2100). In contrast, under the RCP 8.5 scenario, average temperatures are expected to reach 11.01°C, 11.87°C, and 12.89°C, respectively, for the same periods. These results show a more pronounced temperature increase under the RCP 8.5 scenario. The smallest increase—0.53°C—occurs in the near future under RCP 2.6, while the largest increase—2.53°C—occurs in the distant future under RCP 8.5.

An analysis of minimum temperatures indicates that, during the baseline period, the lowest monthly temperature occurred in January, averaging −3.43°C. Under RCP 2.6, the minimum temperatures in January for the near, mid-term, and distant futures are projected to be −2.95°C, −2.76°C, and −2.73°C, respectively, showing increases of at least 0.48°C and up to 0.71°C. Similarly, under RCP 8.5, the minimum January temperatures for the near, mid-term, and distant futures are projected at −2.86°C, −2.15°C, and −1.29°C, indicating respective increases of 0.57°C, 1.28°C, and 2.14°C.

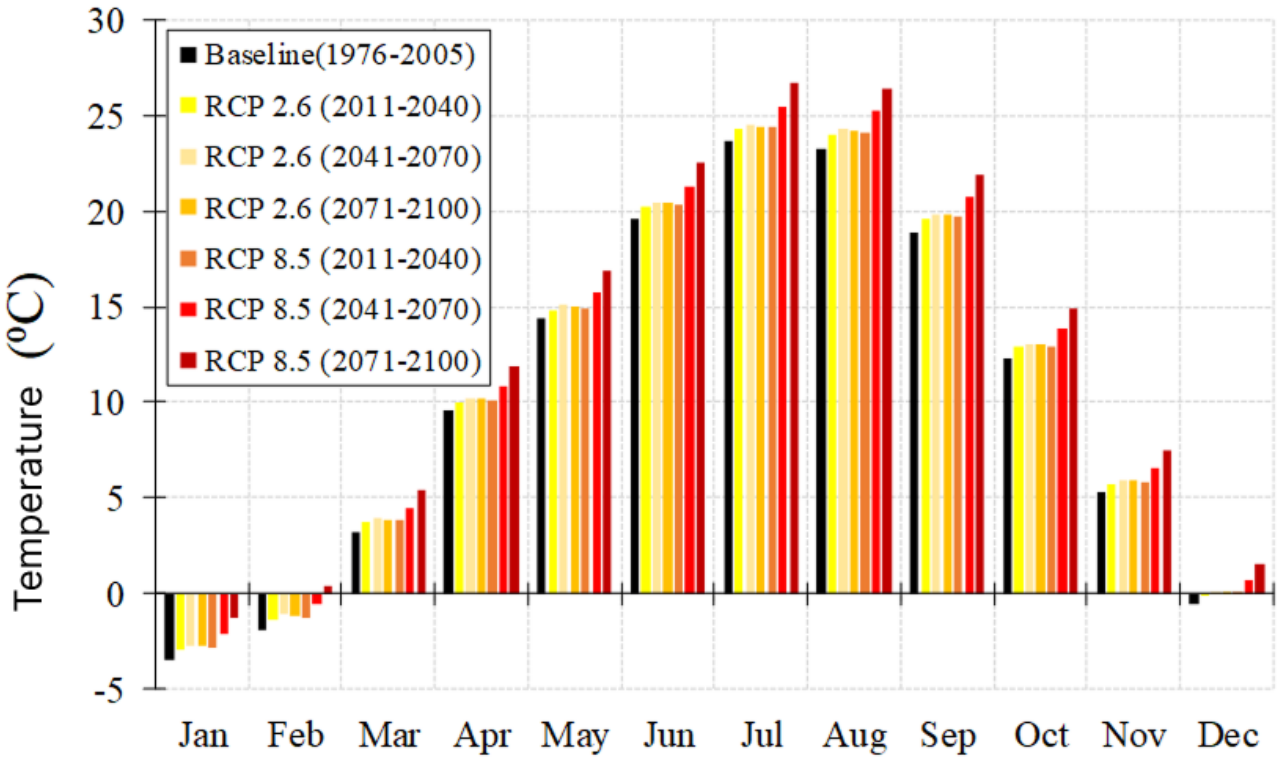

Figure 10. Temperature patterns in the baseline and future periods under different scenarios for the Lake Urmia basin

According to Figure 11, the total annual precipitation in the Urmia basin during the baseline period was 389 mm. Under the optimistic RCP 2.6 scenario, annual precipitation is projected to increase, reaching 395 mm, 401 mm, and 397 mm in the near, mid-term, and distant futures, respectively—representing increases of 1.65%, 3.14%, and 2.18%. However, under the pessimistic RCP 8.5 scenario, there is no change in precipitation in the near future, while decreases of 2.68% and 7.65% are expected in the mid-term and distant futures, respectively.

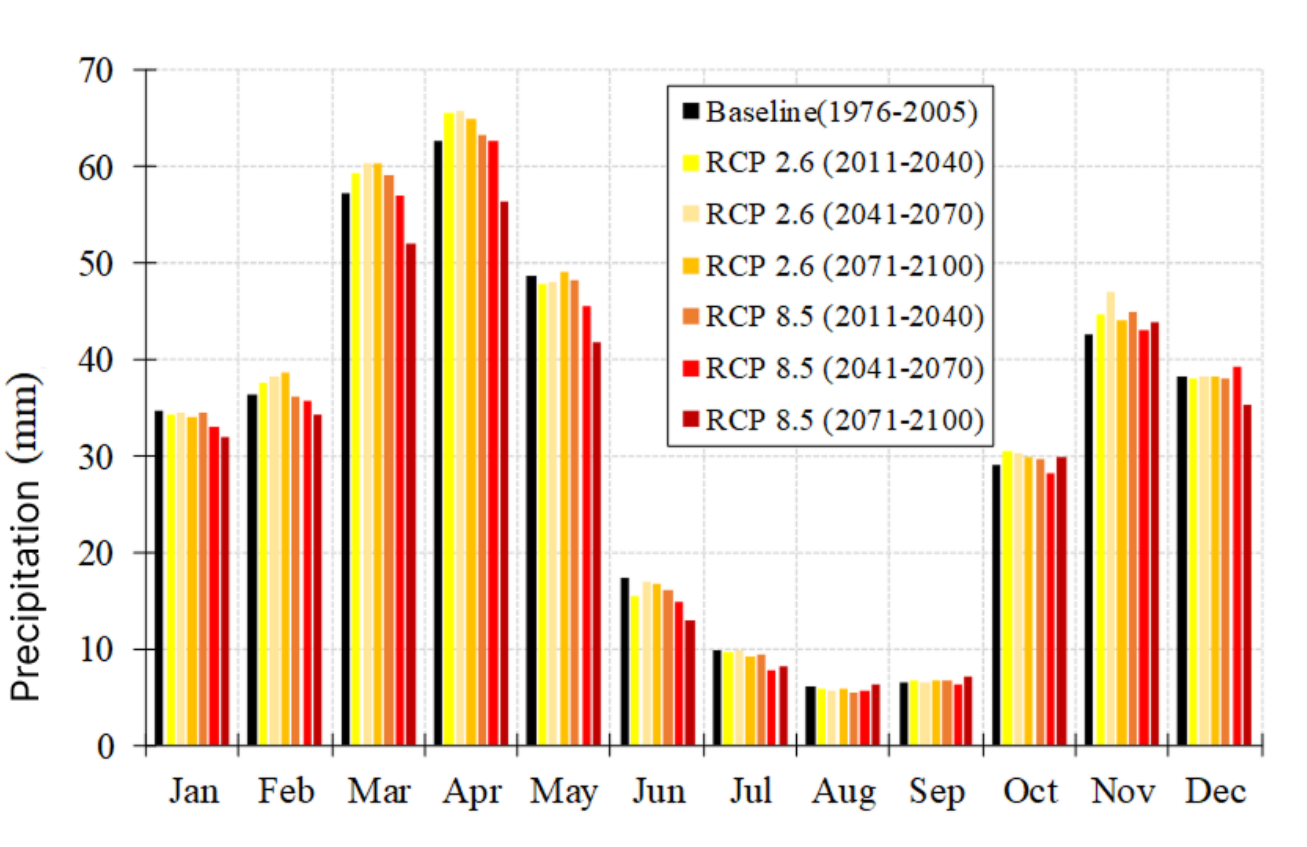

Figure 11. Precipitation patterns in the baseline and future periods under different scenarios for the Lake Urmia basin

3.4. Analysis of Droughts in Future Periods

Figure 12 presents SPI results across different timescales. The SPI-1 and SPI-3 results for short-term droughts indicate a decline in the frequency of normal conditions (WD class) in the future. Under RCP 2.6, the frequency of moderate and severe droughts is projected to decline, whereas under RCP 8.5, the frequency of these droughts increases. The frequency of exceptional droughts (D4) is expected to rise in all future periods under both scenarios. For instance, SPI-3 shows that 6 severe drought events were identified during the baseline period, while 8, 6, and 7 such events are projected under RCP 2.6, and 9, 10, and 13 events under RCP 8.5, for the near (2011–2040), mid-term (2041–2070), and distant (2071–2100) futures, respectively. For medium- and long-term droughts (SPI-6, SPI-9, SPI-12, and SPI-24), the frequency of normal (WD) classes will decline. Overall, under RCP 2.6, the total number of drought events remains relatively unchanged, whereas under RCP 8.5, drought occurrence—particularly from 2071 to 2100—increases significantly.

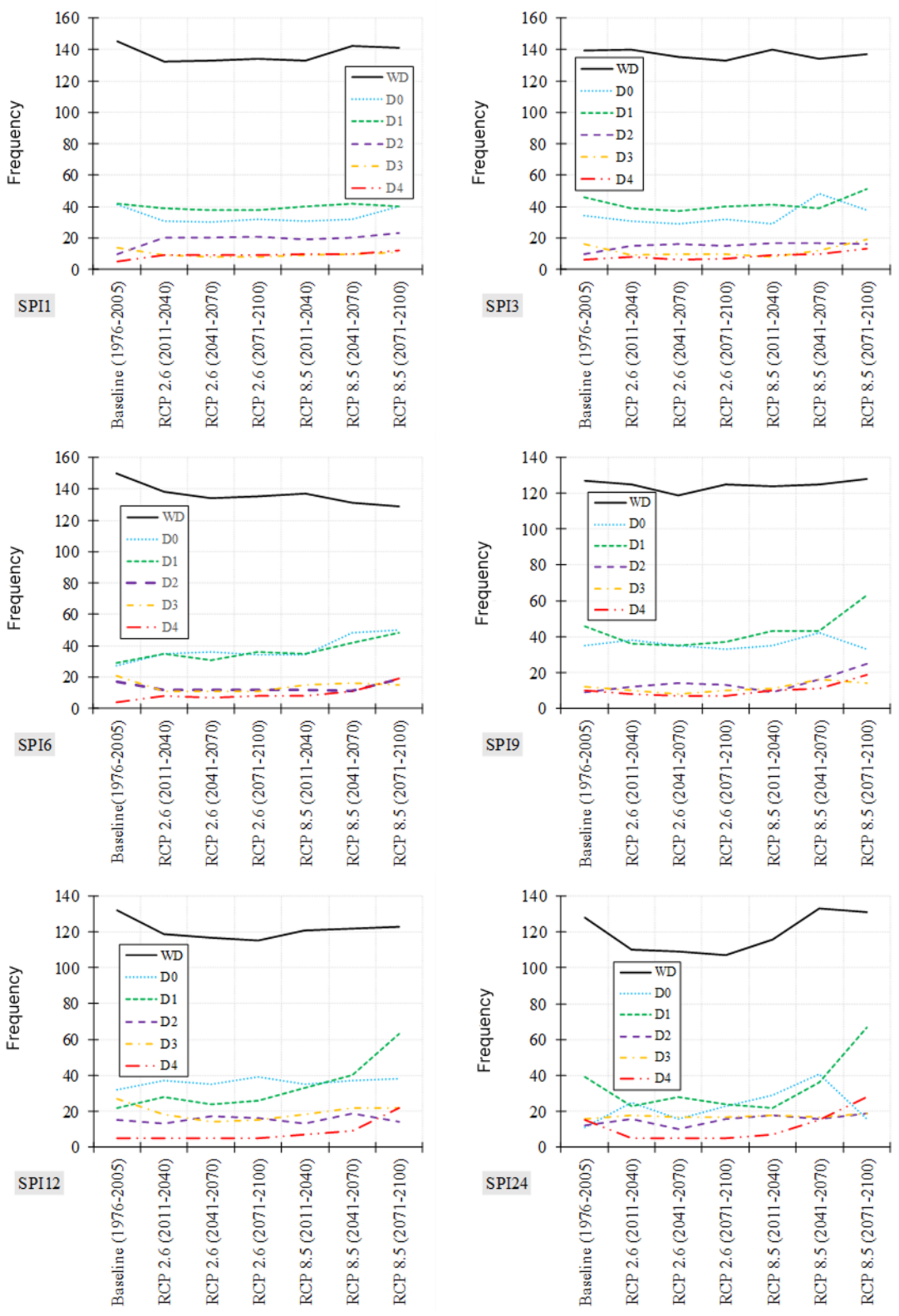

Figure 12. Frequency of drought classes in the baseline and future periods under different scenarios based on the SPI index

Figure 13 illustrates the frequency of drought events based on the SPEI index for the Urmia basin across baseline and future periods. As shown, the frequency of normal conditions (WD) decreases significantly under all future periods and both scenarios, especially under RCP 8.5, leading to increased frequency of droughts across all classes and scenarios. For example, based on SPEI-9, 12 severe drought events (D3) were recorded in the baseline period,

while under RCP 2.6, the number increases to 18, 19, and 19 for the near, mid-term, and distant futures, respectively. Under RCP 8.5, the number of severe drought events rises to 21, 28, and 38 over the same periods—two to three times higher than the baseline. The results show that SPEI identifies more drought events than SPI.

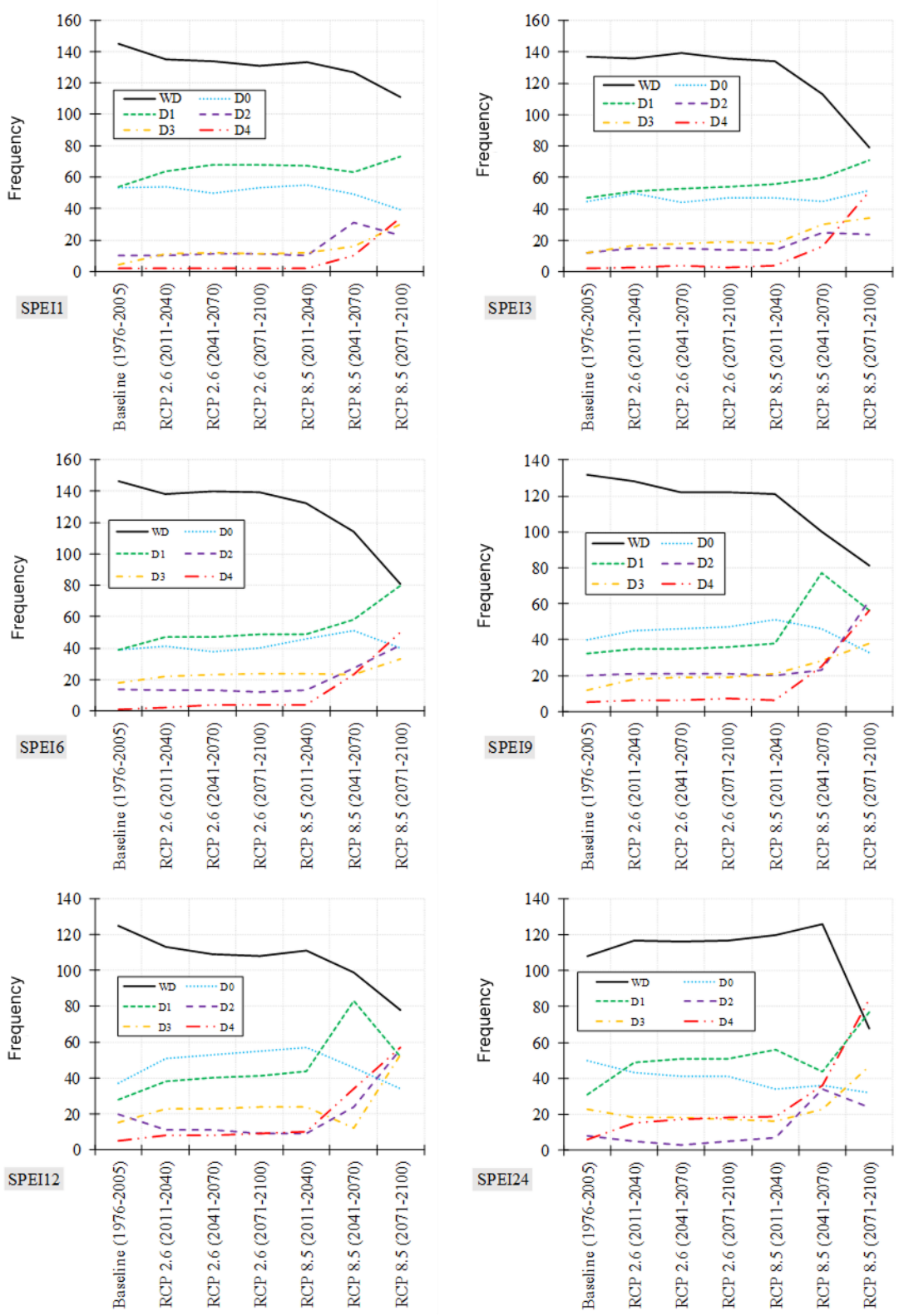

Figure 13. Frequency of drought classes in the baseline and future periods under different scenarios based on the SPEI index

Table 6 presents the results related to the SPI index. According to the data, no clear or consistent pattern is evident in SPI outcomes. For instance, the longest drought period based on SPI-12 during the baseline period is 50 months, while under the RCP 8.5 scenario for the 2071–2100 period, the longest drought duration is 42 months. In the case of SPI-24, the longest drought in the baseline period lasted 93 months, while under RCP 8.5, this duration increases to 110 months.

Table 6. Characteristics of the longest droughts in the baseline and future periods based on different SPI timescales

Scenario	SPI Scale	Mean	Max	Severity	Duration (months)
Baseline (1976–2005)	SPI-1	−1.35	−2.29	−10.79	8
	SPI-3	−1.33	−1.98	−17.25	13
	SPI-6	−1.45	−2.21	−46.25	32
	SPI-9	−1.44	−2.39	−53.33	37
	SPI-12	−1.61	−2.05	−80.29	50
	SPI-24	−1.34	−2.17	−124.58	93
RCP 2.6 (2011–2040)	SPI-1	−0.93	−1.17	−4.64	5
	SPI-3	−1.45	−1.84	−14.46	10
	SPI-6	−1.46	−2.04	−19.00	13
	SPI-9	−1.36	−2.30	−50.47	37
	SPI-12	−1.43	−2.41	−57.37	40
	SPI-24	−1.53	−2.59	−65.75	43
RCP 2.6 (2041–2070)	SPI-1	−0.90	−1.11	−4.49	5
	SPI-3	−1.42	−1.81	−14.17	10
	SPI-6	−1.43	−1.99	−18.60	13
	SPI-9	−1.32	−2.25	−48.82	37
	SPI-12	−1.41	−2.36	−54.85	39
	SPI-24	−1.49	−2.53	−62.44	42
RCP 2.6 (2071–2100)	SPI-1	−0.89	−1.12	−4.46	5
	SPI-3	−1.43	−1.85	−14.31	10
	SPI-6	−1.46	−2.01	−18.97	13
	SPI-9	−1.35	−2.27	−49.97	37
	SPI-12	−1.42	−2.39	−56.77	40
	SPI-24	−1.51	−2.57	−65.09	43
RCP 8.5 (2011–2040)	SPI-1	−0.96	−1.15	−4.81	5
	SPI-3	−1.48	−1.84	−14.77	10
	SPI-6	−1.50	−2.07	−19.55	13
	SPI-9	−1.41	−2.35	−52.35	37
	SPI-12	−1.49	−2.45	−59.60	40
	SPI-24	−1.57	−2.66	−69.08	44
RCP 8.5 (2041–2070)	SPI-1	−1.02	−1.21	−5.10	5
	SPI-3	−1.46	−1.88	−16.07	11
	SPI-6	−1.49	−2.16	−37.18	25
	SPI-9	−1.53	−2.45	−57.98	38
	SPI-12	−1.62	−2.58	−66.25	41
	SPI-24	−1.39	−2.83	−98.77	71
RCP 8.5 (2071–2100)	SPI-1	−0.92	−2.02	−5.51	6
	SPI-3	−1.45	−2.58	−18.85	13
	SPI-6	−1.45	−2.65	−29.05	20
	SPI-9	−1.61	−2.71	−67.56	42
	SPI-12	−1.79	−2.82	−75.29	42
	SPI-24	−1.41	−3.09	−154.55	110

Table 7 presents the SPEI results, which show a more notable pattern. Based on SPEI, the longest duration or greatest severity of droughts in future periods either remains unchanged or increases (except for SPEI-1, where increases occur in all periods). These results indicate that droughts are expected to become more intense and prolonged in future periods. The worst and most severe drought is projected under the RCP 8.5 scenario in the distant future (2071–2100), where the drought duration increases from 65 months in the baseline to 122 months. Additionally, the maximum drought index severity increases from −2.41 in the baseline to −3.74 in the distant future. Stagge et al. (2017)

demonstrated that changes in PET can significantly affect drought severity, which aligns with the findings of this study. Similarly, Lieu et al. (2017), who assessed drought using SPI and SPEI under climate change conditions in China, found that increases in drought intensity and duration are more significant when measured using SPEI rather than SPI—consistent with the present study.

Table 7. Characteristics of the longest droughts in the baseline and future periods based on different SPEI timescales

Scenario	SPEI Scale	Mean	Max	Severity	Duration (months)
Baseline (1976–2005)	SPEI-1	−1.04	−1.43	−5.22	5
	SPEI-3	−1.31	−1.96	−14.36	11
	SPEI-6	−1.35	−2.13	−39.29	29
	SPEI-9	−1.50	−2.32	−62.99	42
	SPEI-12	−1.60	−2.28	−67.35	42
	SPEI-24	−1.39	−2.41	−90.04	65
RCP 2.6 (2011–2040)	SPEI-1	−0.76	−1.12	−4.58	6
	SPEI-3	−1.45	−1.85	−17.44	12
	SPEI-6	−1.47	−2.11	−42.67	29
	SPEI-9	−1.62	−2.36	−68.13	42
	SPEI-12	−1.68	−2.44	−73.78	44
	SPEI-24	−1.24	−2.57	−130.64	105
RCP 2.6 (2041–2070)	SPEI-1	−0.81	−1.21	−4.84	6
	SPEI-3	−1.49	−1.83	−17.87	12
	SPEI-6	−1.51	−2.11	−43.76	29
	SPEI-9	−1.66	−2.38	−69.69	42
	SPEI-12	−1.71	−2.49	−75.37	44
	SPEI-24	−1.27	−2.62	−133.80	105
RCP 2.6 (2071–2100)	SPEI-1	−1.02	−1.42	−7.13	7
	SPEI-3	−1.49	−1.86	−17.83	12
	SPEI-6	−1.51	−2.13	−43.90	29
	SPEI-9	−1.67	−2.38	−69.96	42
	SPEI-12	−1.42	−2.51	−86.81	61
	SPEI-24	−1.29	−2.63	−135.97	105
RCP 8.5 (2011–2040)	SPEI-1	−0.80	−1.16	−4.78	6
	SPEI-3	−1.50	−1.85	−18.00	12
	SPEI-6	−1.44	−2.17	−63.43	44
	SPEI-9	−1.68	−2.41	−70.68	42
	SPEI-12	−1.43	−2.52	−88.67	62
	SPEI-24	−1.32	−2.65	−139.11	105
RCP 8.5 (2041–2070)	SPEI-1	−1.23	−1.68	−9.87	8
	SPEI-3	−1.59	−2.53	−44.42	28
	SPEI-6	−1.73	−2.52	−79.47	46
	SPEI-9	−1.50	−2.73	−120.34	80
	SPEI-12	−1.47	−2.98	−179.00	122
	SPEI-24	−1.75	−3.11	−195.60	112
RCP 8.5 (2071–2100)	SPEI-1	−1.48	−2.08	−20.74	14
	SPEI-3	−1.86	−3.34	−57.61	31
	SPEI-6	−1.72	−3.13	−142.66	83
	SPEI-9	−1.85	−3.39	−230.98	125
	SPEI-12	−2.02	−3.56	−246.24	122
	SPEI-24	−2.28	−3.74	−277.70	122

4. Discussion and Conclusion

The findings of the present study highlight the critical implications of climate change on future drought patterns in the Lake Urmia Basin, utilizing two complementary drought indices—SPI and SPEI—across multiple temporal scales and under two distinct RCP scenarios (2.6 and 8.5). The results demonstrated that the longest drought durations, particularly based on SPI24 and SPEI24, are projected to increase significantly in the distant future (2071–2100), particularly under the pessimistic RCP 8.5 scenario. While SPI indicated irregular trends in drought duration and severity, SPEI consistently showed a marked increase in the frequency, duration, and severity of droughts across all

future periods. For instance, the longest drought duration based on SPEI24 is projected to extend from 65 months in the baseline period to 122 months in the late 21st century under RCP 8.5. Moreover, the severity of droughts intensified sharply, reaching a value of -277.70 for SPEI24, suggesting more extreme climatic events in the basin's future.

This divergence between SPI and SPEI in projecting future drought scenarios underscores the heightened importance of temperature in driving drought conditions. The rising temperatures, particularly under RCP 8.5, have contributed to higher evapotranspiration, exacerbating moisture deficits even when precipitation remains stable or increases slightly. This trend aligns closely with the findings of Vicente-Serrano et al. (2010), who developed SPEI precisely to account for the role of PET in a warming climate and emphasized that temperature-induced drought intensification may go undetected using precipitation-only indices like SPI [2]. Similarly, Lee et al. (2017) demonstrated in their longitudinal study of North Korea that droughts assessed by SPEI displayed greater intensification compared to SPI in response to temperature rises over time, reinforcing the robustness of our findings in the context of semi-arid basins [12].

The findings also resonate with the conclusions drawn by Stagge et al. (2017), who noted increasing divergence in drought indices across Europe, particularly when temperature-driven indicators such as SPEI were considered [11]. This divergence becomes more pronounced over time, which may explain the observed disparity between SPI and SPEI results in this study, especially under RCP 8.5. Furthermore, Funk et al. (2015) provided strong evidence that CHIRPS data, used in this study, effectively capture climatic extremes across Africa and parts of Asia, supporting the reliability of the drought trends derived from these datasets [9]. The predictive results from the GA-SVR model in our research also reflected high accuracy for short lead times (1-step ahead), but showed declining performance as the forecasting horizon increased, a behavior consistent with the findings of Mishra and Desai (2006) and Hosseini-Moghari and Araghinejad (2015), who similarly observed a decrease in drought prediction accuracy with longer forecast horizons [15, 18].

Importantly, the role of temperature was not only reflected in drought indices but also in projected climate variables. Under RCP 8.5, the mean annual temperature is expected to rise by more than 2.5°C by the end of the century, compared to the baseline. Even under the optimistic RCP 2.6 scenario, consistent warming was observed across all future periods. Such warming has been proven to intensify evapotranspiration, thereby increasing drought severity and duration, particularly when precipitation remains constant or decreases. This dynamic supports findings from Morid et al. (2007), who highlighted that temperature plays a dominant role in intensifying droughts, especially in arid regions with high PET sensitivity [16]. Likewise, the significance of PET in amplifying drought severity is supported by the work of Stagge et al. (2015), who found that drought impacts in Europe became more pronounced when temperature was integrated into drought indices [19].

In terms of spatial precipitation trends, while modest precipitation increases were projected under RCP 2.6 for near and mid-term futures, a decline was projected under RCP 8.5 in the mid and long term. These findings parallel those reported by Raziei et al. (2011) and Katiraie-Boroujerdy et al. (2016), who noted that variability and decline in precipitation are more pronounced under higher-emission climate scenarios in Iran [6, 7]. However, the data also indicate that even in scenarios where precipitation remains stable or increases slightly, the rise in temperature alone is sufficient to exacerbate drought severity, as captured by SPEI. This further confirms that temperature has a greater influence on future drought severity than precipitation trends—a conclusion also drawn by Koutsouris et al. (2016) in their study on East African basins [13].

From a methodological perspective, the GA-SVR model proved to be an effective hybrid approach for SPI-based drought forecasting. The advantage of combining evolutionary algorithms with machine learning techniques was evident in the model's ability to handle nonlinearities in climatic time series. This corroborates earlier studies such as DannadeMehr et al. (2014), who used gene-wavelet models for long-lead drought forecasting, and Hosseini-Moghari and Araghinejad (2015), who employed statistical neural networks to enhance monthly drought predictions [17, 18]. The observed trend in our study, where forecast accuracy improved with longer aggregation timescales (e.g., SPI12 and SPI24), is consistent with Wilks' (2011) assertion that temporal aggregation smooths short-term noise and reveals dominant climatic signals more effectively [20].

Another important observation was the drastic increase in drought severity and frequency under RCP 8.5, especially in the distant future. The maximum drought severity value for SPEI24 reached -277.70, which is more than double the baseline severity. Similar patterns have been observed by El

Kenawy and McCabe (2016), who reported multi-decadal increases in drought extremes across Saudi Arabia based on model-based rainfall products [14]. Additionally, the systematic increase in PET-driven droughts in our study supports the findings of Seastedt (2024), who emphasized that climate change not only affects water availability but also has profound public health implications through the amplification of heat and drought extremes [22]. Such projections are not merely theoretical—they have real consequences for ecosystem resilience, agricultural productivity, and water governance.

Furthermore, the role of precipitation dataset accuracy and bias correction was not overlooked. Given the reliance of SPI and SPEI on input precipitation and temperature data, systematic biases in these datasets can significantly affect drought detection. Adam and Lettenmaier (2003) emphasized the need to adjust global gridded precipitation for systematic bias to ensure reliable hydrological modeling [3]. Similarly, Azizi et al. (2016) evaluated several reanalysis datasets over Iran and found considerable inconsistencies among them, reinforcing the need for regional verification [5]. The decision to use ensemble GCM outputs and verified reanalysis datasets (e.g., GPCC, CRU) in this study reflects lessons learned from such foundational works.

Finally, the increasing uncertainty surrounding climate impacts on droughts reinforces the importance of uncertainty modeling in climate-hydrological studies. Lu (2024) highlighted how artificial intelligence can improve climate change mitigation by managing such uncertainty effectively, particularly when integrated with domain-specific indices and models [25]. Moreover, Zhang and Wang (2024) addressed the broader responsibility of institutions and governments to prepare for climate-related damages, particularly in environmentally vulnerable regions like Lake Urmia, where governance, adaptation, and accountability must be integrated [23].

Despite the methodological rigor and integration of hybrid models and climate scenarios, this study is not without limitations. First, the reliance on reanalysis and GCM datasets, although validated and bias-corrected, may still introduce errors due to regional underrepresentation or coarse spatial resolution. Additionally, the study did not account for land-use changes, groundwater extraction, or reservoir operations, all of which may significantly influence hydrological conditions in the basin. Another limitation concerns the extrapolation of the GA-SVR model for longer forecasting horizons, where performance dropped significantly, reducing predictive reliability beyond short-term forecasts. Furthermore, the use of SPEI assumes a fixed PET model, which may not fully capture future changes in vegetation, soil moisture, or wind patterns that influence actual evapotranspiration.

Future studies should incorporate hydrological modeling that includes land use dynamics, irrigation withdrawals, and groundwater interactions to provide a more comprehensive picture of drought vulnerability. Incorporating remote sensing data, such as NDVI or soil moisture indices, could enhance the real-time monitoring of agricultural droughts. Additionally, ensemble machine learning models combining GA-SVR with LSTM or CNN architectures could improve long-term forecasting accuracy. Future research should also explore socioeconomic vulnerability layers, integrating climate data with population density, crop yield, and infrastructure resilience metrics. Moreover, uncertainty quantification techniques, including Monte Carlo simulations and Bayesian inference, should be integrated to assess the confidence intervals of drought projections under each RCP scenario.

Policymakers and regional planners should prioritize drought mitigation strategies based on temperature-sensitive indices like SPEI, given their higher sensitivity to climate change impacts. Water resource management frameworks must be updated to reflect mid- and long-term drought projections under RCP 8.5. Adaptive infrastructure—such as smart irrigation systems and drought-resilient crop planning—should be designed using short-term forecasts from hybrid models. Educational outreach on climate literacy, especially in rural and water-stressed communities, is essential for behavioral adaptation. Lastly, transboundary water governance must be emphasized, as droughts in shared basins like Lake Urmia can have regional ripple effects on ecology, agriculture, and migration.

Authors' Contributions

Authors equally contributed to this article.

Acknowledgments

Authors thank all participants who participate in this study.

Declaration of Interest

The authors report no conflict of interest.

Funding

According to the authors, this article has no financial support.

Ethical Considerations

All procedures performed in this study were under the ethical standards.

References

[1] S. Beguería and S. M. Vicente-Serrano, "SPEI: calculation of the standardised precipitation-evapotranspiration index," ed, 2013.

[2] S. M. Vicente-Serrano, S. Beguería, and J. I. López-Moreno, "A multiscalar drought index sensitive to global warming: the standardized precipitation evapotranspiration index," *Journal of climate*, vol. 23, no. 7, pp. 1696-1718, 2010, doi: 10.1175/2009JCLI2909.1.

[3] J. C. Adam and D. P. Lettenmaier, "Adjustment of global gridded precipitation for systematic bias," *Journal of Geophysical Research: Atmospheres*, vol. 108, no. D9, p. 4275, 2003, doi: 10.1029/2002JD002499.

[4] A. Khalili and J. Rahimi, "High-resolution spatiotemporal distribution of precipitation in Iran: a comparative study with three global-precipitation datasets," *Theoretical and applied climatology*, vol. 118, no. 1-2, pp. 211-221, 2014, doi: 10.1007/s00704-013-1055-1.

[5] G. Azizi, T. Safarrad, H. Mohammadi, and H. Faraji Sabokbar, "Evaluation and comparison of reanalyzed precipitation data for use in Iran," *Physical Geography Research*, vol. 48, no. 1, pp. 33-49, 2016.

[6] P. S. Katiraie-Boroujerdy, N. Nasrollahi, K. L. Hsu, and S. Sorooshian, "Quantifying the reliability of four global datasets for drought monitoring over a semiarid region," *Theoretical and applied climatology*, vol. 123, no. 1-2, pp. 387-398, 2016, doi: 10.1007/s00704-014-1360-3.

[7] T. Raziei, I. Bordi, and L. S. Pereira, "An application of GPCC and NCEP/NCAR datasets for drought variability analysis in Iran," *Water Resources Management*, vol. 25, no. 4, pp. 1075-1086, 2011, doi: 10.1007/s11269-010-9657-1.

[8] U. Schneider, A. Becker, P. Finger, A. Meyer-Christoffer, and B. Z. Rudolf, "GPCC Full Data Reanalysis Version 7.0 at 0.5: Monthly Land-Surface Precipitation from Rain-Gauges built on GTS-based and Historic Data," ed, 2015.

[9] C. Funk *et al.*, "The climate hazards infrared precipitation with stations-a new environmental record for monitoring extremes," *Scientific data*, vol. 2, p. 150066, 2015, doi: 10.1038/sdata.2015.66.

[10] I. P. D. J. Harris, P. D. Jones, T. J. Osborn, and D. H. Lister, "Updated high-resolution grids of monthly climatic observations-the CRU TS3. 10 Dataset," *International Journal of Climatology*, vol. 34, no. 3, pp. 623-642, 2014, doi: 10.1002/joc.3711.

[11] J. H. Stagge, D. G. Kingston, L. M. Tallaksen, and D. M. Hannah, "Observed drought indices show increasing divergence across Europe," *Scientific Reports*, vol. 7, no. 1, p. 14045, 2017, doi: 10.1038/s41598-017-14283-2.

[12] S. H. Lee, S. H. Yoo, J. Y. Choi, and S. Bae, "Assessment of the Impact of Climate Change on Drought Characteristics in the Hwanghae Plain, North Korea Using Time Series SPI and SPEI: 1981-2100," *Water*, vol. 9, no. 8, p. 579, 2017, doi: 10.3390/w9080579.

[13] A. J. Koutsouris, D. Chen, and S. W. Lyon, "Comparing global precipitation data sets in eastern Africa: a case study of Kilombero Valley, Tanzania," *International Journal of Climatology*, vol. 36, no. 4, pp. 2000-2014, 2016, doi: 10.1002/joc.4476.

[14] A. M. El Kenawy and M. F. McCabe, "A multi-decadal assessment of the performance of gauge-and model-based rainfall products over Saudi Arabia: climatology, anomalies and trends," *International Journal of Climatology*, vol. 36, no. 2, pp. 656-674, 2016, doi: 10.1002/joc.4374.

[15] A. K. Mishra and V. R. Desai, "Drought forecasting using feed-forward recursive neural network," *Ecological Modelling*, vol. 198, no. 1, pp. 127-138, 2006, doi: 10.1016/j.ecolmodel.2006.04.017.

[16] S. Morid, V. Smakhtin, and K. Bagherzadeh, "Drought forecasting using artificial neural networks and time series of drought indices," *International Journal of Climatology*, vol. 27, no. 15, pp. 2103-2111, 2007, doi: 10.1002/joc.1498.

[17] A. DannadeMehr, E. Kahya, and M. Özger, "A gene-wavelet model for long lead time drought forecasting," *Journal of Hydrology*, vol. 517, pp. 691-699, 2014, doi: 10.1016/j.jhydrol.2014.06.012.

[18] S. M. Hosseini-Moghari and S. Araghinejad, "Monthly and seasonal drought forecasting using statistical neural networks," *Environmental Earth Sciences*, vol. 74, no. 1, pp. 397-412, 2015, doi: 10.1007/s12665-015-4047-x.

[19] J. H. Stagge, I. Kohn, L. M. Tallaksen, and K. Stahl, "Modeling drought impact occurrence based on meteorological drought indices in Europe," *Journal of Hydrology*, vol. 530, pp. 37-50, 2015, doi: 10.1016/j.jhydrol.2015.09.039.

[20] D. S. Wilks, *Statistical methods in the atmospheric sciences*. Academic press, 2011, p. 627.

[21] I. Khusniyawati, "The Learning Activities of RBL-STEM: Prototyping a Water-Powered Lamp to Enhance Students' Climate Change Literacy," *World Journal of Advanced Research and Reviews*, vol. 22, no. 2, pp. 2174-2184, 2024, doi: 10.30574/wjarr.2024.22.2.1671.

[22] H. Seastedt, "Impact of Urban Biodiversity and Climate Change on Children's Health and Well Being," *Pediatric Research*, 2024, doi: 10.1038/s41390-024-03769-1.

[23] J. Zhang and Y. Wang, "On the Liability of Small Island States to Compensate for Loss and Damage Associated With Climate Change Impacts," *Legal Science in China and Russia*, no. 6, pp. 135-144, 2024, doi: 10.17803/2587-9723.2023.6.135-144.

[24] Z. Cao, S. X. Chen, T. Dong, and E. Lee, "Climate Change Uncertainty and Supply Chain Financing," *The British Accounting Review*, p. 101423, 2024, doi: 10.1016/j.bar.2024.101423.

[25] L. Lu, "In-Depth Analysis of Artificial Intelligence for Climate Change Mitigation," 2024, doi: 10.20944/preprints202402.0022.v1.